ADVANCED FUNCTIONAL MATERIALS
www.afm-journal.de

Automated, Ultra-Fast Laser-Drilling of Nanometer Scale Pores and Nanopore Arrays in Aqueous Solutions

*Tal Gilboa, Eran Zvuloni, Adam Zrehen, Allison H. Squires, and Amit Meller**

The ability to quickly and reliably fabricate nanoscale pore arrays in ultra-thin membranes such as silicon nitride (Si_xN) is extremely important for the growing field of nanopore biosensing. Laser-based etching of thin Si_xN membranes immersed in aqueous solutions has recently been demonstrated as a method to produce stable functional pores. Herein, the principal mechanism governing material etching and pore formation using light is investigated. It is found that the process is extremely sensitive to the relative content of Si over N atoms in the amorphous membrane, produced by chemical vapor deposition. Commonly, Si_xN membranes are made to be Si-rich to increase their mechanical stability, which substantially reduces the material's bandgap and increases the density of Si-dangling bonds. Hence, even minimal batch-to-batch variation may lead to remarkably different etch rates. It is shown that higher Si content results in orders of magnitude faster etching rates. This rate is further accelerated in an alkaline environment allowing on-demand controlled nanopore formation in about 10 s time even at low laser radiation intensities. These results highlight that photoactivation of the Si_xN by the incident beam is critical to the chemical etching process and can be used to readily produce nanopore arrays at any specific location.

1. Introduction

Nanopore bio-sensing is one of the fastest growing areas in single molecule analysis and in the past two decades has been applied to study a variety of biological systems.[1] For example, nanopore sensing has been developed and utilized for DNA sequencing, direct probing of single DNA–protein complexes, and label-free protein characterization.[2–8] Solid-state nanopores (ssNPs) fabricated in ultra-thin planar membranes are an important class of nanopores that are typically crafted in solid, inorganic materials, such as silicon nitride, titanium, or aluminum oxides, as well as 2D membranes, such as graphene or MoS_2.[9–15] To produce nanoscale pores with high control over the nanopore dimensions, researchers have extensively employed high-end electron or ion microscopy tools, such as transmission electron microscopy (TEM) and focused ion beam milling.[15,16] Nonetheless, these techniques have not yet been shown to be effective in preparing large nanopore arrays in which subsequently individual nanopores are addressed electrically, particularly in cases where µm-scale nanopore to nanopore pitch is desired. Optical sensing, on the other hand, may significantly simplify the paralleled sensing from nanopore arrays as it does not involve the incorporation of dedicated pairs of electrodes for each nanopore.[17,18] Recently, a lithographic procedure involving reactive ion etching (RIE) was used to fabricate nanopore arrays, but the approach yielded nanopores ≈15 nm in diameter, too large for many sensing applications.[19] The helium ion milling approach, although successful for sub-5 nm nanopore arrays, is prohibitively expensive and unavailable to many laboratories.[14,20] A low-cost alternative to ssNP fabrication is controlled dielectric breakdown (CBD),[21–23] which to fabricate nanopore arrays requires that each intended nanopore site be electrically isolated from the others, whether by an integrated microfluidic channel or by a microscale liquid contact.[24,25]

We recently reported on a method for direct, in situ laser-based membrane-thinning and fabrication of ssNPs in the range of just a few nanometers in freestanding silicon nitride (Si_xN) membranes (x = 0.75 for stoichiometric Si_3N_4).[26] Requiring just a mW-intensity laser and a confocal microscope, nanopores could be fabricated at any arbitrary position and in any quantity. These nanopores were shown to exhibit noise levels matching their TEM-drilled counterparts and translocate both nucleic acids and proteins. Subsequent reports have exploited the thinning effect of the laser drilling in Si_xN membranes in order to accelerate CBD pore creation.[27,28] However, the physical process governing laser-drilling in thin, water-immersed membranes, particularly in the absence of any dielectric breakdown application, has remained obscure. Specifically, the relative contributions of direct heating versus polarization of the thin membrane by the laser light, have to date remained unclear. While heating has already been implicated in speeding up the chemical dissolution of the Si_xN membrane,[27] the role of charge generation at the membrane due to incident irradiation has yet to be elucidated. At the same time, laser-induced

T. Gilboa, E. Zvuloni, A. Zrehen, Prof. A. Meller
Department of Biomedical Engineering
Technion–IIT
Haifa 32000, Israel
E-mail: ameller@technion.ac.il
Dr. A. H. Squires
Department of Chemistry
Stanford University
Stanford, CA 94305, USA
The ORCID identification number(s) for the author(s) of this article can be found under https://doi.org/10.1002/adfm.201900642.
DOI: 10.1002/adfm.201900642

microchemistry in semi-conductors has widely been attributed to the optical creation of an electron–hole pair and the migration of the latter to the solid–liquid interface where it catalyzes chemical interactions.[29] Undoubtedly, a better understanding of the physical basis of the light-activated drilling process is not only fundamentally interesting, but could also potentially improve selection of the material and environment conditions to enable ultra-fast and accurate nanopore drilling.

Amorphous Si_xN films are typically produced using a chemical vapor deposition (CVD) process, tuned to form silicon-rich membranes with respect to stoichiometric Si_3N_4, resulting in low-stress thin films.[30] The Si:N ratio (denoted x) only slightly alters the material's refractive index, but it greatly affects the abundance of the Si dangling bonds,[31] and in turn the photoluminescence (PL) spectrum produced by the film,[32] as the latter involves photo-activated electron excitation and relaxation. Indeed, previous studies have revealed that free-standing Si_xN films suspended in aqueous solutions produce strong, red-shifted PL emission when irradiated by blue-green lasers (i.e., 488–532 nm), and that the PL intensity is highly dependent on Si:N ratio.[32,33] Moreover, e-beam irradiation of the membrane preferentially removes nitrogen atoms, producing a locally Si-enriched area exhibiting a red-shifted PL spectrum and strong photo-reactivity, even at sub-mW laser powers.[33,34] These results prompted us to hypothesize that materials composed of slightly different Si:N ratios would result in dramatically altered laser drilling characteristics. To check this hypothesis, we systematically fabricated a series of Si_xN films with different Si:N ratios. We characterized the material properties for each batch, including the Si:N composition and energy bandgaps using electron energy loss spectroscopy (EELS) and energy dispersive X-ray spectroscopy (EDS), and studied the laser drilling mechanism under various excitation wavelengths and solution pH. Our results point to a highly Si:N composition- and pH-dependent mechanism that is clearly photo-activated. Importantly, we show that at high Si:N ratios and alkaline conditions, we can drill functional nanopores in <10 s at laser excitation powers that are roughly an order of magnitude smaller than those employed in previous reports.[26,27] This enables controlled in situ laser fabrication of nanopore arrays with arbitrary patterns within minutes.

2. Results and Discussion

2.1. The Si_xN Membrane Etching Rate Strongly Depends on the Si:N Ratio

Material composition analysis is not routinely performed as part of the low pressure CVD (LPCVD) process because it involves delicate elemental spectroscopy. Instead, the material's index of refraction is often used as a proxy for the Si:N composition, in which a higher index of refraction corresponds to a higher content of Si over N in Si_xN membranes.[30] Notably, however, small changes in the index of refraction correspond to significantly different Si:N compositions, preventing fine control of the Si:N ratio, and resulting in significant batch-to-batch variations. While these variations may be too small to affect e-beam or ion-beam nanopore drilling methods, we readily detect their effect on laser-based drilling as reported here. We produced four wafer batches using the same LPCVD instrument which had slightly different Si:N compositions, characterized by their indices of refraction (2.15, 2.20, 2.29, and 2.42, as measured by an ellipsometer). To monitor the Si_xN membrane thinning prior to pore creation, we used a custom-made confocal microscope equipped with multiple laser excitation lines and two spectrally resolved emission channels coupled to two avalanche photodiodes (APDs; see **Figure 1**a and the Experimental Section). After positioning the membrane at the focus of the laser spot,[35] we measured the PL intensity time-trace during laser irradiation. We typically observed a fast PL intensity reduction followed by a slower decay associated with the gradual decrease in membrane thickness and the formation of a Gaussian-shaped etch profile. The ion current and PL were simultaneously monitored during laser irradiation, and pore formation was signaled by an abrupt jump in the ion current. We also inspected each nanochip before and after the laser process under white light illumination to locate visible thinning of the membrane (see the Experimental Section).

We first compare the membrane thinning and NP drilling kinetics of two 45 nm thick Si_xN membranes (488 nm, 6 mW measured at sample plane) having slightly different indices of refraction (n = 2.20 and n = 2.29, Figure 1b,c). Although the difference in the reflectivity of the different batches (calculated as $R = (n_s - n_w)^2/(n_s + n_w)^2$ where n_s and n_w are the Si_xN and water indices, respectively) is less than 2%, they were affected differently by laser irradiation: the membrane with the higher index of refraction formed a thinned area and a pore through the 45 nm thick membrane within 2 min, while the membrane with a slightly lower index of refraction did not form a pore even after >40 min of continuous irradiation, and displayed significantly higher initial PL. Inspecting these chips under white light illumination (right-hand panels on Figure 1b,c) showed that in both cases, membrane thinning occurred. These experiments were performed at pH 7 in high salt (Tris-HCl buffer, 1 M KCl) and reproduced many times (N > 100 times).

The striking difference in the thinning and drilling time between the two chip types, which only differed slightly in their Si:N compositions, prompted us to hypothesize that the nanopore drilling process is photo-activated. Attempts to thermally induce membrane etching by suspending the membranes in the same buffer (Tris-HCl pH 7, 1 M KCl) at 90 °C for over 60 min produced negligible or no etching at all of either Si_xN membranes as measured by ellipsometry (Figure S1, Supporting Information). This may suggest that the drilling process requires an electronic transition in the Si-rich membranes, which cannot be provided by heating alone. Indeed, nanochips with an even higher index of refraction (n = 2.42) could be drilled in less than 2 min at even lower excitation laser power (2.8 mW, Figure 1d). Attempting to drill the n = 2.42 chips at 6 mW laser power resulted in near instantaneous (less than a second) formation of a large pore, which was hard to control.

In order to establish the relationship between the Si_xN membrane indices of refraction and the Si:N composition, we analyzed the materials using both EELS and EDS; see the Experimental Section. Each chip was cleaned using argon plasma before measuring the EELS or EDS spectrum. We employed dual EELS measurements to obtain both low loss and

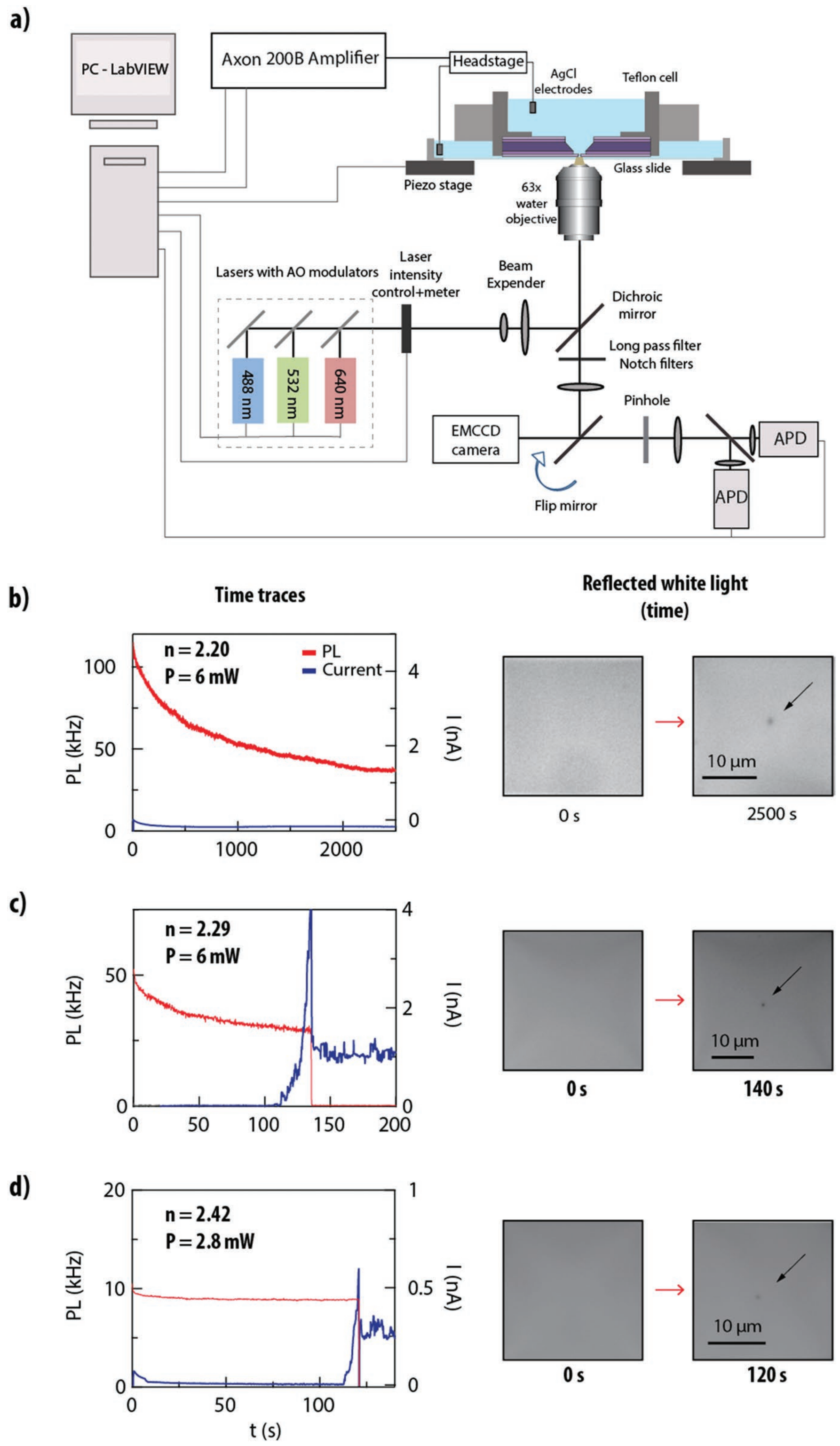

Figure 1. Nanopore fabrication by laser-etching. a) Schematic illustration of the electro-optical apparatus used for laser-assisted nanopore drilling. b–d) Laser thinning in three membranes with different indices of refraction: $n = 2.20$, 2.29, 2.42 for b), c), and d), respectively. Laser intensity is equal in all cases. Left: PL and current traces during etching. A sudden incline in the current trace indicates pore formation. For the $n = 2.20$ membrane, no pore was formed even after 2500 s, whereas for the $n = 2.29$, 2.42 membranes pores were formed after 140 and 120 s, respectively. Right: images of the membrane before and after etching. In all cases a black spot (indicated by a black arrow) appears in the later images, where less light was reflected, indicating a thinner region. The formation of thinner membrane regions is reflected in the PL traces (left) which decrease in all cases regardless of pore formation. These experiments were reproduced more than 100 times each.

core loss data, in order to estimate both the material thickness (using the low loss spectrum) and the material composition (using the core loss spectrum). The atomic percentage of each material was also measured at the same position using EDS. The thickness estimation indicated similar thicknesses for all tested chips in the range of 44–46 nm. While systematic differences between EELS and EDS in measuring the Si:N ratio are expected based on previous literature,[36] our results (**Figure 2**a) show a consistent trend and agree very well with a previously employed empirical model (red solid lines) predicting that

$$\mathrm{Si}:\mathrm{N} = \frac{3n + 3n_\infty - 6n_{3/4}}{4n_\infty - 4n} \tag{1}$$

where n_∞ is the refractive index of pure Si and $n_{3/4}$ is the refractive index of Si_3N_4 (reported theoretical values are $n_\infty = 3.86$, $n_{3/4} = 1.99$).[30] Fitting each of the measurements with the model resulted in the following parameter values: $n_\infty = 3.995$, $n_{3/4} = 1.964$ for the EELS and $n_\infty = 3.683$, $n_{3/4} = 1.740$ for the EDS (dashed lines). These measurements indicate that on average, the atomic Si:N ratio ranges from about 0.9 to 1.5 for the range of indices from 2.15 to 2.42, respectively, representing significantly larger Si content as compared to the stoichiometric value of Si_3N_4 (0.75). EELS-based bandgap measurements of the chips with refractive indexes of 2.15 and 2.42 showed, as described before, that higher refractive index results in a smaller bandgap (Figure S2, Supporting Information).[37] Using the lower bandgap Si-rich chips we were able to drill nanopores using a green (532 nm) laser with intensity of 5 mW in less than 2 min (Figure S3, Supporting Information).

The fact that Si-rich membranes were much more readily drilled using focused light prompted us to further study their optical properties. We focused our attention on the PL emission of the membranes, as this phenomenon is strictly related to photon absorption and photon emission associated with electron excitation/relaxation (unlike scattering). To avoid inducing any material etching, we reduced the laser power by three orders of magnitude to ≈7 µW and measured the PL emission in two spectrally defined emission bands (550 nm < Ch1 < 650 nm, Ch2 > 650 nm; see the Experimental Section). In Figure 2b, we show the total PL emission (green markers and line) measured for these samples, as well as the ratio of the red-band emission over the total emission (red markers and line). Our results show significantly lower apparent PL intensities for the higher Si_xN indices of refraction: Changing the index of refraction from 2.15 to 2.42 resulted in roughly seven-fold PL reduction in the measured visible band. This result initially appeared to be counterintuitive; the Si_xN membrane bandgap energy slightly decreases with increasing Si content, which should allow more efficient electron excitation from the valance to conduction bands prior to their relaxation and the emission of a red-shifted PL.[37] However, as the material becomes successively more Si-rich, the density of the Si dangling bonds is known to increase, providing additional energy relaxation pathways involving lower energy photon emissions.[38] Indeed, we observe a systematic red-shifting of the PL at the higher Si:N ratio (Figure 2b, red curve). Noticeably, the lower energy photons associated with these transitions are expected to be outside of the photon counter measurement band. Consequently, these processes would substantially reduce the apparent PL measured in the visible emission band.

2.2. Si_xN Membrane Etching is Accelerated Under Alkaline Conditions

The strong dependency of the Si_xN thinning and nanopore drilling on the Si:N composition suggests that the etching mechanism involves a photochemical reaction. At low irradiation intensities, and specifically for Si-rich material, the laser-induced temperature rise in the water-submersed thin film appears to be less critical than electronic excitation. In this regime, the enhancement in etch rate can be related to the generation of electron–hole pairs within the Si_xN surface and charge transfer at the liquid–solid interface.[29] At the water interface, the dissolution rate of a silica-like material is expected to be strongly affected by pH since the hydroxyl ion is a catalyst for the hydrolysis that underlies the dissolution process.[39] We therefore hypothesized that the etch rate and subsequent pore formation rates could be further accelerated under alkaline conditions.[27]

To investigate this possibility, we performed a set of experiments to measure the membrane etching rate and pore formation as a function of pH, under different laser irradiation intensities. We performed two complimentary measurements: 1) using white-light microscopy we measured the membrane thinning rate by comparing the transmitted light intensity before and after irradiation of a laser for a fixed length of time. 2) Additionally, we used the PL intensity as a proxy for the etching process and characterized its kinetics (Figure S4, Supporting Information). Our results show a clear and consistent trend: Under acidic pH, the thinning process is slowed down significantly, as evidenced by nearly imperceptible changes in the transmitted light intensity. In fact, only under strong laser intensity could we visually discern thinning at all. The PL kinetics measurements were only weakly dependent on the laser intensity at this pH. In contrast, under alkaline conditions (i.e., pH 10 or 12) the drilling process is highly accelerated. Specifically, we observe membrane thinning even at extremely low laser power irradiation down to just a few mW and the PL kinetics show strong dependency on the laser power.

To quantify the thinning rate under different conditions, we irradiated the same chip for a fixed length of time at different laser intensities. Then we switched buffers as indicated (see the Experimental Section), and the measurements were repeated several times. In **Figure 3**a, we show typical results of the white light image (100X magnification) at 4 pH values, measured using the same laser intensity. We can clearly observe increased thinning under alkaline conditions (pH 10–12) and little to no thinning at pH 4. To quantify the result, we show in Figure 3b the normalized intensity changes as a function of laser power, measured at $t = 120$ s. Our results can be approximated by a linear dependence of the etching rate on the laser power. From the slopes of the curve we obtain the following ratios for pH 7, 10, and 12 as compared with the pH 4 slope used a reference: 2.3 ± 0.24, 8.46 ± 0.6, and 10 ± 0.61, respectively. These results indicate that thinning can occur at high pH, even at low laser power. In addition, high pH buffer allows fast initiation

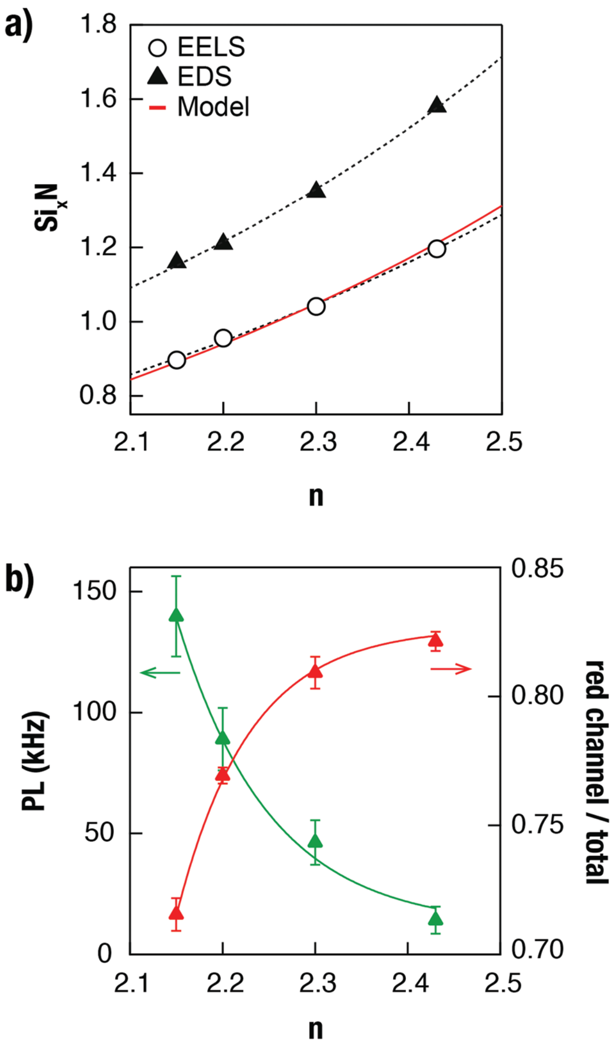

Figure 2. Membranes characterization. a) Material composition as a function of the refractive index measured using EDS (triangles) and EELS (circles). Red curve represents the theoretical model with reported theoretical values of n_∞ = 3.86, $n_{3/4}$ = 1.99. A higher refractive index indicates higher percentage of silicon in the membrane. Fitting each of the measurements with the theoretical model resulted in the following parameter values: $n_\infty = 3.9949$, $n_{3/4} = 1.9638$ for the EELS and $n_\infty = 3.6827$, $n_{3/4} = 1.7401$ for the EDS (solid black lines). b) Average PL values for four different membrane types (n = 2.15, 2.2, 2.29, 2.42) of similar thickness (44–46 nm). A lower refractive index produced higher PL (green marks). The results are fitted to exponential curves (green solid line). Red triangles present the ratio of the red-band emission over the total emission, which increases as the refractive index increases. This is associated with a red-shift of the PL at the higher Si:N ratio. Each measurement was repeated using four membranes of each type.

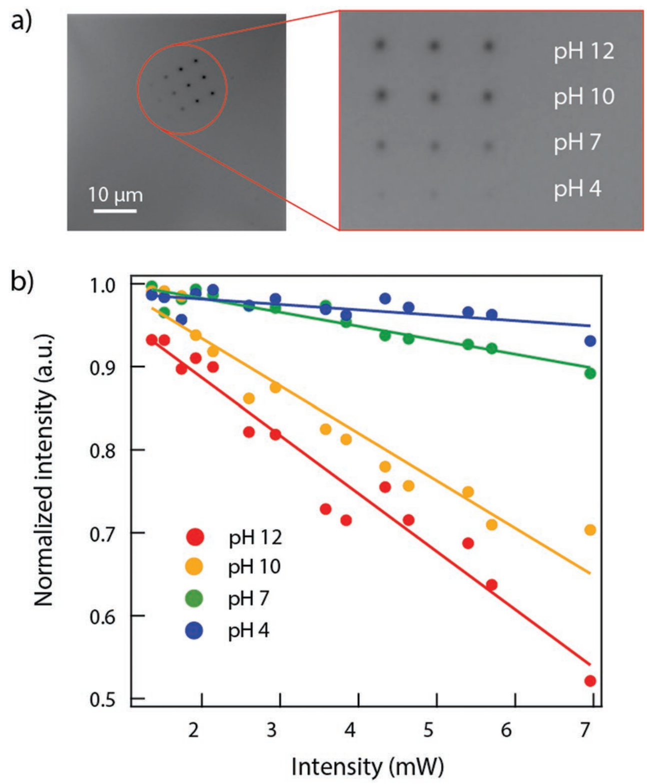

Figure 3. Membrane thinning as a function of the solution pH. a) Reflected white light image of a chip (n = 2.29) before laser exposure (488 nm) and after exposing it for 1 min at different pH levels and 1 M KCl (each measurement was repeated three times). b) The normalized intensity is the change in reflected white light according to (signal-background)/background for each condition (four different pH levels) after exposing the chip for 2 min as a function of the laser intensity. Solid lines for each pH imply a linear dependence of the etch rate on laser power.

of the thinning process, which could provide excellent conditions to drill nanopores at high speed (Figure S4, Supporting Information).

2.3. Ultra-Fast Nanopore Drilling in Si-Rich Membranes

The strong dependency of thinning on pH and material composition encouraged us to further analyze and characterize this process in order to achieve controlled, ultra-fast, nanopore drilling at low laser intensities. We first immersed a chip with refractive index of 2.29 in high pH buffer (pH 10), exposed it to a 488 nm laser of 7 mW for varying durations, and created a thickness map of the exposed region using EELS. As expected, the thickness maps presented in **Figure 4**a show that longer illumination results in increased thinning. This is further demonstrated by comparing the line scans in the middle of each thinned region (Figure S5, Supporting Information). Integrating over this line scan shows a similar trend to the PL measurement during thinning, indicating that the PL can be used to approximate changes in thickness and membrane composition (Figure 4b). High-magnification TEM images revealed that an exposure of ≈15 s was enough to create a ≈5 nm pore in the center of the Gaussian-shaped thin region (see left inset in Figure 4b). But further irradiation of the surface under these conditions resulted in multiple pores, as can be seen at ≈20 s or at longer time points. Hence, a current gradient threshold should be set to automatically shut off the laser at the onset of nanopore formation to minimize the likelihood of multiple pores, as was done for fabricating a nanopore array (Figure 6).

A drilling trace using a similar chip (refractive index of 2.29), pH 10 buffer, and 488 nm laser with intensity of 6 mW in which

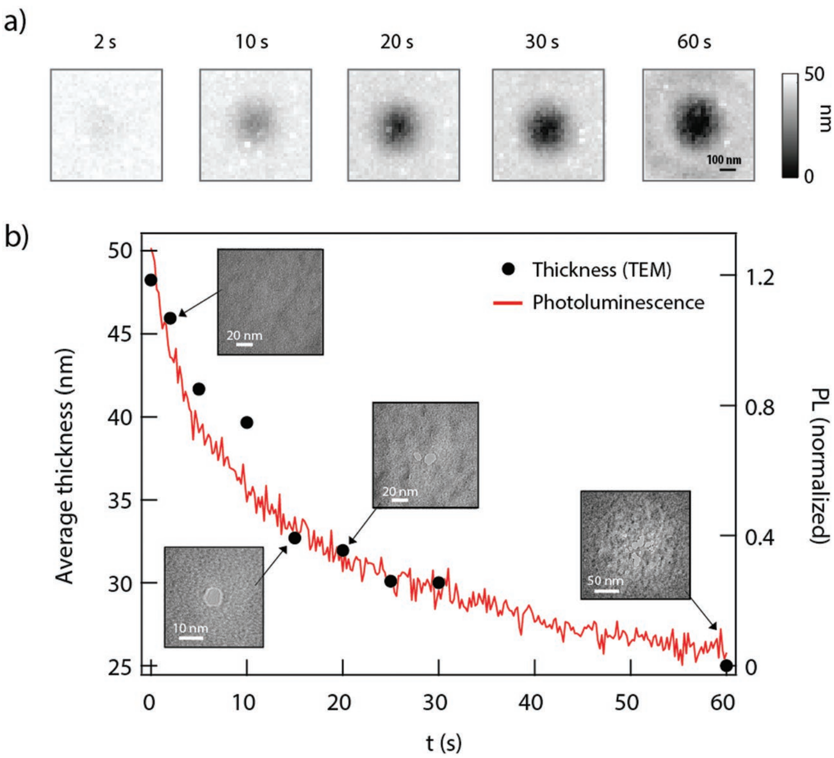

Figure 4. Characterization of the ultra-fast drilling process. a) STEM thickness map of a thin region created using increasing laser exposure durations. Conditions: 488 nm, 7 mW, 1 M KCl, pH 10. A longer exposure duration results in a thinner membrane. b) Normalized, integrated thickness for x-line scans taken in the middle of the thickness maps for each exposure duration (black circles), and the PL trace as a function of time (red curve). Inset: high magnification TEM images for selected thin regions. After laser exposure of 15 s a single ≈5 nm pore was created in the middle of the Gaussian-shaped thin region. Longer exposures resulted in the formation of multiple pores.

pore formation was detected electrically in less than 15 s is presented in **Figure 5**a. To check the nanopore functionality, we immediately changed the buffer to a pH 7 buffer, added DNA sample (300 bp), and measured translocations (Figure 5b,c). The pore diameter and effective thickness were calculated according to the average fractional blockage level (0.81 ± 0.01) and conductance (19.1 nS) as previously described.[26] The calculated results suggest that the pore diameter is 5 ± 0.4 nm with an effective thickness of 5 ± 1 nm. A scatterplot of the dsDNA translocation events and concatenated ionic current trace showing sample translocation events are presented in Figure 5.

2.4. An Automated In Situ Fabrication of Nanopore Arrays Using Direct Laser Etching

The ability to quickly form arrays of nanopores placed at any chosen locations is extremely important for future use of nanopores in high-throughput applications including nucleic-acid sequencing and protein identification. Both the means to electrically address each individual nanopore in an array, as well as parallel optical sensing, have been proposed and developed.[17,20] Taking advantage of the ultra-fast, in situ drilling process presented in Section 2.3, we developed a simple hardware-controlled system for drilling an arbitrary array of pores. Specifically, drilling was automated by providing a list of coordinates and a current gradient threshold. After focusing the laser on the membrane at low intensity, 150 mV was applied across the membrane, and the PL and current were measured in real time. After focusing, the piezo stage moved the membrane to the first coordinate in the list, and the laser intensity was increased to 7 mW. Once the change in current increased above the current gradient threshold, the laser was switched off and the piezo stage moved to the next point (**Figure 6**a, top), where the laser was switched on again. In this way the drilling process could stop immediately when a predetermined increase in current was detected (Figure 6a, bottom).

Figure 6 displays an example of an array of 25 nanopores drilled in ≈6.5 min. Panel a displays time traces of the laser intensity (top), PL, and current (bottom, red and blue lines, respectively). As can be seen, all pores formed in less than 20 s, where small variations in the drilling time are mainly due to changes in the laser focus. Histograms of the drilling time and the change in the total current for each drilled pore are presented in Figure 6b. The nanopore array was inspected by wide-field fluorescence microscopy using Ca^{2+}-activated fluorophores. Upon applying a +300 mV bias, 24 out of 25 fluorescent spots appeared at the expected nanopore locations as Ca^{2+} ions were drawn through the nanopores and reacted with the Ca^{2+} indicator dye (Figure 6c, middle panel). The fluorescent spots disappeared when the opposite voltage bias was applied (Figure 6b, left panel). To estimate the variation in pore sizes, we integrated the fluorescence intensities of each spot. A histogram of the result is shown in Figure 6b (right) and is well-fit by a Gaussian distribution.

3. Conclusions

Laser-etching of amorphous silicon nitride membranes suspended in aqueous solutions has proven to be a highly versatile method for controlled nanoscale pore fabrication.[26] Focusing on the photoactivity of the incident light, we show here that both the etching and nanopore drilling kinetics can be accelerated by orders of magnitudes using higher Si to N ratio membranes, measured as a slight increase in their index of refraction. Specifically, a change in the index of refraction of Si_xN membranes from ≈2.20 to ≈2.42 corresponded to a transition from a non-drilling membrane, even after nearly an hour of exposure, to nearly instantaneous nanopore formation. We hypothesize that photoinduced membrane polarization leading to surface charging may accelerate hydroxyl-driven etching in solution.

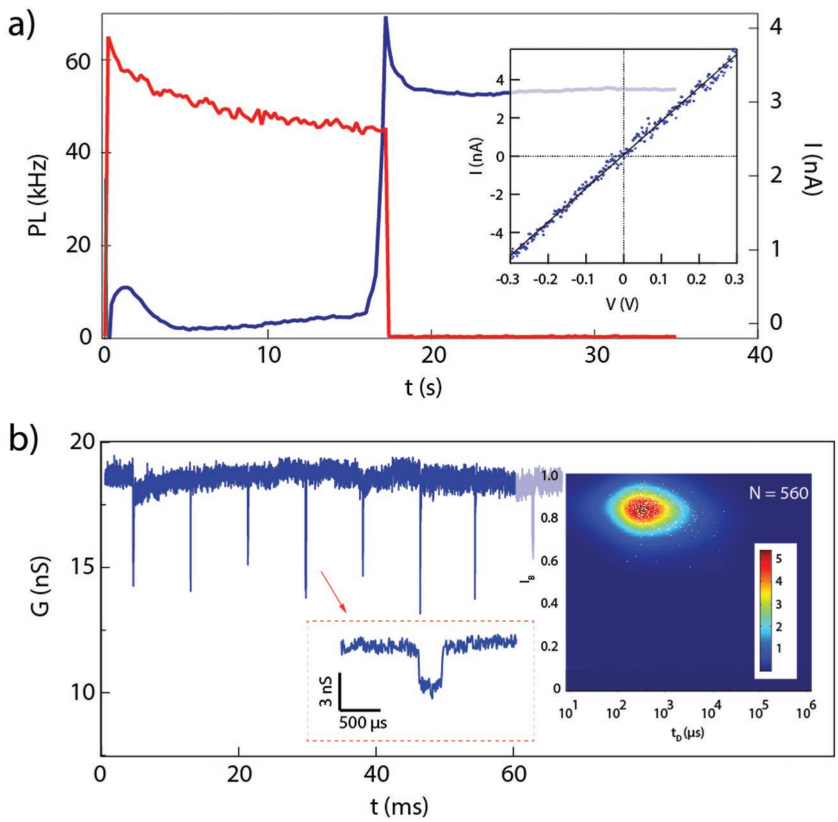

Figure 5. DNA translocations measured using a fast-drilled nanopore. a) PL and current traces of a pore drilled in ≈15 s. The laser was turned on at $t = 0$, as indicated by an abrupt PL increase. The PL decays over time as the membrane is thinned until pore formation, signaled by an increase in the electrical current. Conditions: 1 M KCl, pH 10, 300 mV, 488 nm wavelength with intensity of 7 mW. The inset shows the current–voltage (I–V) curve for this nanopore after the buffer was changed to pH 7 and the open pore current stabilized. b) Concatenated dsDNA (300 bp) translocation events with a zoomed in plot of an event, and the scatter plot of the blocked current ($I_B = I_{blocked}/I_{open}$) versus the dwell time t_D of all the events ($N = 560$).

Indeed, when the solution pH was raised to pH 10 we observed ultra-fast pore formation, even when using a low laser power that could not etch the material at normal pH. Following optimization, drilling yielded individual 5 nm pores in 15 s from a starting 45 nm thick substrate. Such ultra-fast drilling can be utilized for preparing nanopore arrays at any arbitrary position, limited only by diffraction. As a proof-of-principle, we designed a fully automated feed-back-controlled protocol for drilling a 25 nanopore array in about 7 min without any user-intervention.

Electro-optical sensing using ssNPs is an important and growing area of research.[18] The addition of an optical sensing modality to the ohmic measurement expands the application space for nanopore sensing, as has recently been demonstrated for DNA methylation quantification and polypeptide discrimination.[12,35] Here, we find that the Si-rich membranes, which react much more readily to light, also produce less PL in the visible to near-infrared range. Analysis of the PL emission indicates that the emission is red-shifted outside our measurement range, which is potentially less disruptive for visible range single-molecule fluorescence sensing. While additional measurements will be needed to fully characterize this effect, involving IR spectroscopy, the immediate implication is that these laser-drilled nanopores can be applied to multi-color electro-optical single-molecule sensing.

4. Experimental Section

Chip Fabrication and Assembly: Nanopore chips were fabricated from a 4″ double-side polished, 350 µm thick silicon wafer coated with 500 nm of thermal SiO_2 (Silicon Valley Microelectronics, CA USA). 50 nm thick low-stress silicon nitride (Si_xN) layer was deposited on both sides using LPCVD with different NH_3/SiH_2Cl_2 gas ratios, resulting in different refractive indexes ranging from 2.15 to 2.43. The refractive index was then measured by ellipsometry (Film Sense, FS-1). Next, direct-write photolithography (MicroWriter ML3, DMO) was used to pattern the windows and dice lines on the resist. A hard mask was created using RIE (Diener Electronic) followed by buffered oxide etch (BOE) to remove the SiO_2 and expose the Si layer. The wafer was then immersed in KOH at 65 °C for up to 20 h followed by a second round of BOE to open up a freestanding Si_xN membrane. Each chip was cleaned by piranha before usage (3:1 H_2SO_4:H_2O_2), vacuum dried, and mounted onto a Teflon holder with Ecoflex 5 (Smooth-ON, Reynolds Advanced Materials) silicone rubber. The chip was then placed in a Teflon cell equipped with a quartz cover-slide bottom. The position of the cell was controlled using a 3D nanopositioner stage (Physik Instrumente, P-561.3CD).

Experimental Setup: A custom-made three-color confocal setup was used for the electro-optical measurements as depicted in Figure 1a and described in detail elsewhere.[33] The lasers were focused to a diffraction-limited spot at the membrane surface using a high NA objective (Zeiss Apochromat 63x/1.15). The emitted light was collected using the same objective, filtered using the appropriate long pass and notch filters (Semrock), and focused on either an EMCCD camera (ANDOR, iXon 887) or a 100 µm pinhole (Thorlabs). Light passing through the pinhole was collimated and split using a dichroic mirror (Semrock) with center wavelengths of $\lambda = 650$ nm and focused onto two APDs (Perkin Elmer SPCM-AQR-14). The emitted light was attenuated using an ND3 filter during thinning and drilling to protect the APDs. Photon counting from the APDs was sampled at 500 kHz (DAQ NI-6602). The PL presented throughout the paper was a summation of the red (>650 nm) and green (550–650 nm) channels. Ionic current was measured by *cis/trans*-immersed Ag/AgCl electrodes connected to a high-bandwidth amplifier (Axon 200B) sampled at 125 kHz (DAQ NI-6514) and filtered at 10 kHz. The two cards were triggered simultaneously via a hardware connection and were fully controlled by custom LabVIEW software.

TEM Imaging: High-resolution images were acquired with an FEI Titan Themis Cs-Correct HR-S/TEM. The low loss energy spectrum was measured in scanning transmission electron microscopy (STEM) in increments of 20 nm and was used to automatically generate relative thickness maps using Digital Micrograph software (Gatan).

Composition Analysis: Chemical mapping of the Si_xN membranes was performed using EDS (Dual Bruker XFlash6) and STEM based on core-loss EELS. The EDS quantification was done using Velox (Thermo Fisher) and EELS quantification was done using the Digital Micrograph software (Gatan).

DNA Translocation Experiments: For the translocation experiment, the chip was immersed in a pH 7 buffer (in buffer, 1 M KCl, 40 × 10^{-3} M

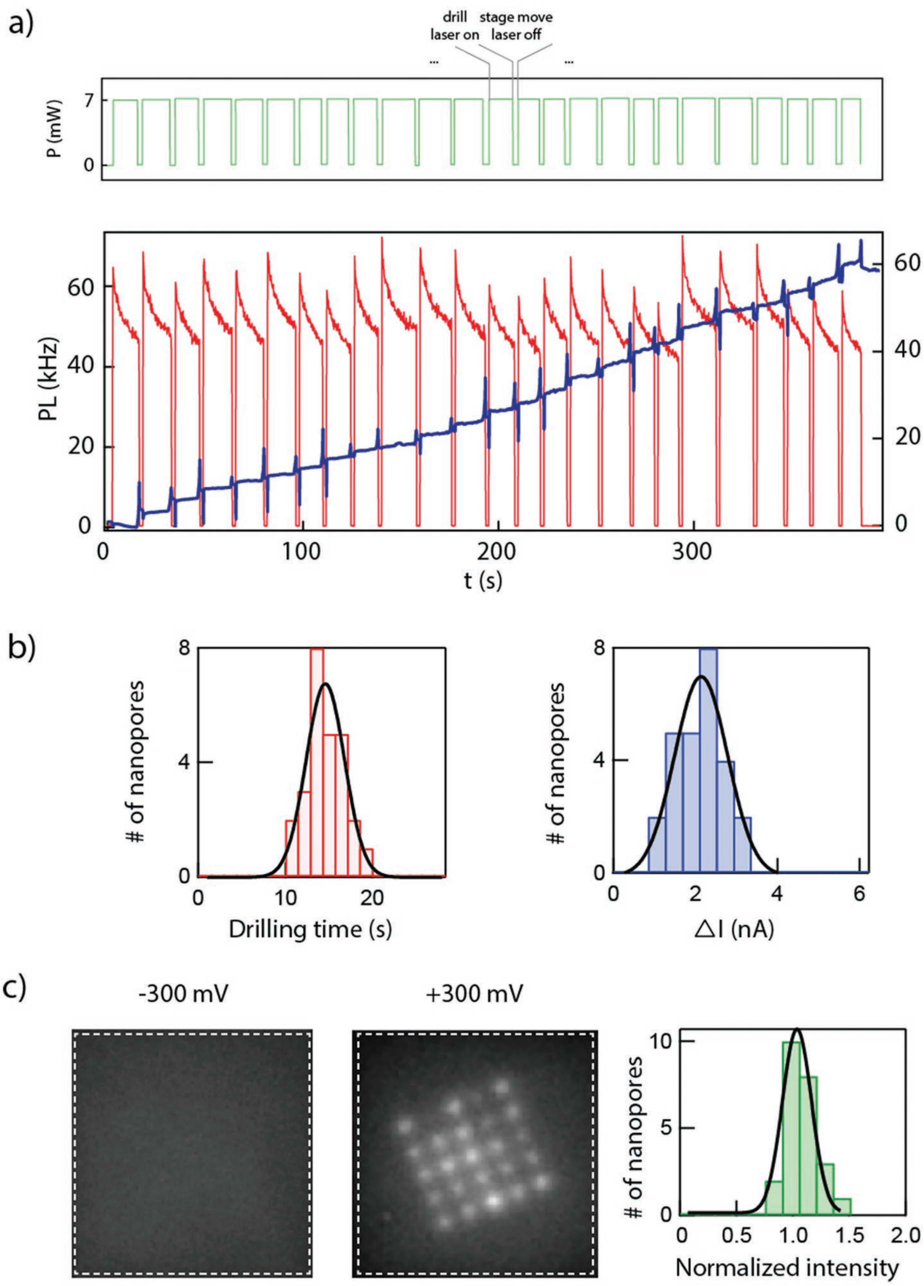

Figure 6. Fast drilling of nanopores array using a focused laser beam. a) Top: laser intensity time trace during nanopore array drilling. The laser power is switched automatically on and off for each drilling event, followed by controlled movement of the piezo stage to the next coordinate. Bottom: PL (red) and current (blue) traces of an array of 25 pores drilled in ≈7 min. When the current rapidly increases, the laser is automatically turned off and the PL drops. b) Histograms of the drilling time and the change of current for each pore, and Gaussian fitting for each histogram (13.6 ± 3.1 s, 1.9 ± 0.9 nA). c) Wide-field illumination images of the entire membrane using 488 nm laser. Calcium (Ca^{+2}) activated fluorophores are used for verifying the creation and position of the nanopore array. At 300 mV Ca^{+2} passes through the pore and binds to Fluo-4, resulting in a fluorescence spot at the thin region (middle panel). The spot disappears when the bias is reversed to −300 mV (left panel). The membrane position is outlined by a white dashed line. The histogram in the right panel describes the normalized intensity distribution of the 25 pores. Black curve is a Gaussian fit (0.97 ± 0.18).

Tris-HCl, 1×10^{-3} M ethylenediaminetetraacetic acid) and 300 mV was applied until the open pore current stabilized. 300 bp dsDNA was added to the *cis* chamber at a concentration of 1×10^{-9} M. Translocation events were monitored and recorded using an Axon 200B filtered at 100 kHz and custom LabVIEW software. An offline analysis program was used to analyze each event separately to extract the amplitude block and dwell time for each translocation.

Automated Nanopore Drilling: Custom software (LabVIEW) was used to automatically drill either a single or multiple pores according to the input coordinates (x,y) list and a current gradient threshold. 150 mV potential was applied across the membrane and the current was monitored in real time. The piezoelectric stage was moved to each coordinate, where the laser was switched on until the current threshold was reached. The laser was then switched off, stopping the drilling. As a preliminary stage to this process, the laser was focused at the ($x = 0, y = 0$) coordinate at low intensity. The nanopores array was validated using Ca^{+2}-based imaging as previously described.[40]

pH Experiments: Four 1 M KCl buffers with different pH levels were prepared: 20×10^{-3} M sodium acetate for pH 4, 20×10^{-3} M Tris for pH 7, 20×10^{-3} M sodium bicarbonate for pH 10, and KOH-based buffer for pH 12. The buffers' refractive index was measured using a refractometer (Rudolph, J257) and was found to be similar for the four solutions (Table S1, Supporting Information). For measuring the dependency of etching in pH, the membrane was immersed in each buffer solution and was exposed to 2 min of laser illumination of increasing intensities. The chip was washed (Milli-Q) and dried before exchanging the buffer. White light images of the membrane were taken before and after the laser exposure using an EMCCD camera and were used to compute the change in reflection through each etched spot (ImageJ and MATLAB). Laser intensity was controlled using an ND filter and monitored using a power meter (Thorlabs).

Supporting Information

Supporting Information is available from the Wiley Online Library or from the author.

Acknowledgements

T.G. and E.Z. contributed eually to this work. The authors acknowledge help from the Cornell Nanoscale Science and Technology Facility. The authors are grateful to Dr. Yaron Kauffmann from the Technion Electron Microscopy Center (MIKA) for his assistance in the FEI Titan Themis operation including composition analysis using EDS and EELS, bandgap measurements, and creation of high-resolution thickness maps. The authors acknowledge the financial support from the BeyondSeq consortium (EC program 63489 to A.M.) and i-Core program of the Israel Science Foundation (1902/12 to A.M.).

Conflict of Interest

The authors declare no conflict of interest.

Keywords

Direct laser drilling, Nanopore arrays, Solid-state Nanopores, Si dangling bonds

Received: January 21, 2019
Revised: March 11, 2019
Published online:

[1] B. M. Venkatesan, R. Bashir, *Nat. Nanotechnol.* **2011**, *6*, 615.
[2] D. Branton, D. W. Deamer, A. Marziali, H. Bayley, S. A. Benner, T. Butler, M. Di Ventra, S. Garaj, A. Hibbs, X. Huang, S. B. Jovanovich, P. S. Krstic, S. Lindsay, X. S. Ling, C. H. Mastrangelo, A. Meller, J. S. Oliver, Y. V. Pershin, J. M. Ramsey, R. Riehn, G. V. Soni, V. Tabard-Cossa, M. Wanunu, M. Wiggin, J. A. Schloss, *Nat. Biotechnol.* **2008**, *26*, 1146.
[3] C. Plesa, S. W. Kowalczyk, R. Zinsmeester, A. Y. Grosberg, Y. Rabin, C. Dekker, *Nano Lett.* **2013**, *13*, 658.
[4] A. H. Squires, T. Gilboa, C. Torfstein, N. Varongchayakul, A. Meller, *in Methods in Enzymology*, Vol. *582* (Eds.: M. Spies, Y. R. Chemla), Academic Press, San Diego, CA **2017**, pp. 353–385.
[5] M. Wanunu, J. Sutin, B. McNally, A. Chow, A. Meller, *Biophys. J.* **2008**, *95*, 4716.
[6] I. Nir, D. Huttner, A. Meller, *Biophys. J.* **2015**, *108*, 2340.
[7] A. Squires, E. Atas, A. Meller, *Sci. Rep.* **2015**, *5*, 11643.
[8] A. Singer, M. Wanunu, W. Morrison, H. Kuhn, M. Frank-Kamenetskii, A. Meller, *Nano Lett.* **2010**, *10*, 738.
[9] G. Danda, P. Masih Das, Y.-C. Chou, J. T. Mlack, W. M. Parkin, C. H. Naylor, K. Fujisawa, T. Zhang, L. B. Fulton, M. Terrones, A. T. C. Johnson, M. Drndić, *ACS Nano* **2017**, *11*, 1937.
[10] K. Liu, J. Feng, A. Kis, A. Radenovic, *ACS Nano* **2014**, *8*, 2504.
[11] G. F. Schneider, S. W. Kowalczyk, V. E. Calado, G. Pandraud, H. W. Zandbergen, L. M. K. Vandersypen, C. Dekker, *Nano Lett.* **2010**, *10*, 3163.
[12] R. Wang, T. Gilboa, J. Song, D. Huttner, M. W. Grinstaff, A. Meller, *ACS Nano* **2018**, *12*, 11648.
[13] C. Dekker, *Nat. Nanotechnol.* **2007**, *2*, 209.
[14] D. Xia, C. Huynh, S. McVey, A. Kobler, L. Stern, Z. Yuan, X. S. Ling, *Nanoscale* **2018**, *10*, 5198.
[15] M. J. Kim, M. Wanunu, D. C. Bell, A. Meller, *Adv. Mater.* **2006**, *18*, 3149.
[16] A. J. Storm, J. H. Chen, X. S. Ling, H. W. Zandbergen, C. Dekker, *Nat. Mater.* **2003**, *2*, 537.
[17] B. N. Anderson, O. N. Assad, T. Gilboa, A. H. Squires, D. Bar, A. Meller, *ACS Nano* **2014**, *8*, 11836.
[18] T. Gilboa, A. Meller, *Analyst* **2015**, *140*, 4733.
[19] D. V. Verschueren, W. Yang, C. Dekker, *Nanotechnology* **2018**, *29*, 145302.
[20] F. Sawafta, B. Clancy, A. T. Carlsen, M. Huber, A. R. Hall, *Nanoscale* **2014**, *6*, 6991.
[21] K. Briggs, H. Kwok, V. Tabard-Cossa, *Small* **2014**, *10*, 2077.
[22] H. Kwok, K. Briggs, V. Tabard-Cossa, *PLoS One* **2014**, *9*, e92880.
[23] I. Yanagi, H. Hamamura, R. Akahori, K. I. Takeda, *Sci. Rep.* **2018**, *8*, 10129.
[24] C. E. Arcadia, C. C. Reyes, J. K. Rosenstein, *ACS Nano* **2017**, *11*, 4907.
[25] R. Tahvildari, E. Beamish, K. Briggs, S. Chagnon-Lessard, A. N. Sohi, S. Han, B. Watts, V. Tabard-Cossa, M. Godin, *Small* **2017**, *13*, 1.
[26] T. Gilboa, A. Zrehen, A. Girsault, A. Meller, *Sci. Rep.* **2018**, *8*, 9765.
[27] H. Yamazaki, R. Hu, Q. Zhao, M. Wanunu, *ACS Nano* **2018**, *12*, 12472.
[28] C. Ying, J. Houghtaling, O. M. Eggenberger, A. Guha, P. Nirmalraj, S. Awasthi, J. Tian, M. Mayer, *ACS Nano* **2018**, *12*, 11458.
[29] D. Bäuerle, *Laser Processing and Chemistry*, Springer Science & Business Media, Berlin **2013**.
[30] J. G. E. Gardeniers, H. A. C. Tilmans, C. C. G. Visser, *J. Vac. Sci. Technol., A* **1996**, *14*, 2879.
[31] J. Robertson, W. L. Warren, J. Kanicki, *J. Non-Cryst. Solids* **1995**, *187*, 297.
[32] F. Giorgis, C. Vinegoni, L. Pavesi, *Phys. Rev. B* **2000**, *61*, 4693.
[33] O. N. Assad, N. Di Fiori, A. H. Squires, A. Meller, *Nano Lett.* **2015**, *15*, 745.
[34] N. Di Fiori, A. Squires, D. Bar, T. Gilboa, T. D. Moustakas, A. Meller, *Nat. Nanotechnol.* **2013**, *8*, 946.
[35] T. Gilboa, C. Torfstein, M. Juhasz, A. Grunwald, Y. Ebenstein, E. Weinhold, A. Meller, *ACS Nano* **2016**, *10*, 8861.
[36] J. M. Titchmarsh, *Ultramicroscopy* **1989**, *28*, 347.
[37] J. Park, S. Heo, J. G. Chung, H. Kim, H. Lee, K. Kim, G. S. Park, *Ultramicroscopy* **2009**, *109*, 1183.
[38] S. V. Deshpande, E. Gulari, S. W. Brown, S. C. Rand, *J. Appl. Phys.* **1995**, *77*, 6534.
[39] E. Laarz, B. V. Zhmud, L. Bergström, *J. Am. Ceram. Soc.* **2000**, *83*, 2394.
[40] A. Zrehen, T. Gilboa, A. Meller, *Nanoscale* **2017**, *9*, 16437.

